ISSN: 2639-7536

Research Article

Petroleum and Chemical Industry International

Zinc Ferrite ($Znfe_2O_4$) For Environmental Remediation

Sana Kausar Ashfaque Ahmad[1], Chetan R. Yewale[1], Rajendra V Wagh[1,2], Vikas V Deshmane[3], Sajid Naeem[4], Umesh J Tupe[5], and Arun V Patil[1,6*]

[1]*Department of Physics and Research Centre, MGV's MSG Arts, Science and Commerce College, Malegaon, Dist: Nashik, (Affiliated to Savitribai Phule Pune University), India*

[2]*MVP's Arts, Commerce and Science College, Nandgaon, At-Post- Nandgaon Dist: Nashik, (Affiliated to Savitribai Phule Pune University), India*

[3]*Department of Physics, SICES Degree College of Arts, Science and Commerce (Affiliated with University of Mumbai), India*

[4]*Department of Applied Sciences, Maulana Mukhtar Ahmad Nadvi Technical Campus, India*

[5]*Department of Electronic Science, Vidya-Amrut Dnyan Pratishthan's Arts, Science and Commerce College, Shirsondi, Tal- Malegaon, Dist: Nashik (Affiliated to Savitribai Phule Pune University), India*

[6]*Department of Physics, MGV's, Arts, Science and Commerce College, Manmad, Dist. Nashik, (Affiliated to Savitribai Phule Pune University), India*

***Corresponding Author**

Arun V Patil, Department of Physics, MGV's, Arts, Science and Commerce College, (Affiliated to Savitribai Phule Pune University), India

Submitted: 2026, Jan 27; **Accepted:** 2026, Feb 16; **Published:** 2026, Feb 27

Citation: Ahmad. S. K. A., Yewale. C. R., Wagh. R. V., Deshmane. V.V., Naeem. S. et al. (2026). Zinc Ferrite ($Znfe_2O_4$) For Environmental Remediation. *Petro Chem Indus Intern, 9*(1), 01-13.

Abstract

If the pollutants are successfully identified, the air pollution can be addressed. The extraordinary qualities of spinel ferrites can be used for this purpose. The goal of the current work was to create spinel ferrite and evaluate its optical and structural characteristics. This study investigates the use of $ZnFeO_4$ nanoparticles (NPs) generated by the precipitation process for static gas sensing applications. Thick films of $ZnFe_2O_4$ were fabricated utilizing an economical screen-printing method. We examined these films utilizing field effect scanning electron microscopy (FESEM), energy dispersive x-ray analysis (EDAX), x-ray diffraction (XRD), ultra-violet visible (UV-Vis) spectroscopy, Fourier transform infrared spectroscopy (FTIR), and Raman analysis to assess their shape, composition, crystalline structure, optical characteristics, and functional groups, respectively. The electrical and gas sensing characteristics of the $ZnFe_2O_4$ films were examined utilizing a half-bridge circuit and a static gas sensing device. The electrical properties, including resistivity, temperature coefficient of resistance (TCR), and activation energy, were evaluated. The resistivity and TCR were measured at 10.4267.8 Ω.m and −0.00191 °C-1, respectively, signifying the material's semiconducting characteristics. The films

were evaluated for their gas sensing capabilities in the presence of oxidizing and reducing gases, such as liquefied petroleum gas (LPG), ethanol, nitrogen dioxide (NO_2), carbon dioxide (CO_2), and methane (CH_4). The $ZnFe_2O_4$ films demonstrated the highest sensitivity of 87.52% to LPG at temperature of 120°C. The films exhibited a swift response time of 12 s and a recovery duration of 83 s upon exposure to LPG. The results highlight the potential of $ZnFe_2O_4$ as a viable material for economical and effective LPG gas sensors.

Keywords: Spinel Ferrite, Gas Sensor, Selectivity, Sensitivity, Temperature Coefficient

1. Introduction

The Comprehensive Environmental Pollution Index (CEPI) was developed by the Central Pollution Control Board (CPCB), Government of India to assess environmental quality in 88 industrial clusters. Out of these clusters, 43 are classified as Critically Polluted Areas (CPAs) and 32 as Severely Polluted Areas (SPAs) [1]. Air toxics, a category of low-concentration contaminants, can induce health effects upon exposure, frequently stemming from motor vehicle emissions and specific commercial and industrial activities [2]. 99% of the global population is exposed to air pollution exceeding WHO standards, with low- and middle-income countries at the worst risk. Ambient air pollution causes 4.2 million deaths globally. The 2001 census estimates sewage generation from Class I cities and Class II towns at 29,129 MLD, anticipated to increase to 33,212 MLD with a 30% decadal growth in urban population [3]. These act as air pollution contributors which includes methane, ethane etc. [1]. This underscores the necessity for effective gas sensors. Chemo resistive sensors are an effective technology for gas detection.

The effectiveness of the gas sensor depends upon the choice of material, synthesis method adopted, synthesis parameters, and the additives used. Techniques including sol-gel, hydrothermal, co-precipitation, microwave-assisted, and combustion methods produce spinel ferrites, allowing for regulation of particle size, shape, and crystallinity. The sol-gel process improves purity and homogeneity, whereas hydrothermal and microwave procedures facilitate the fast synthesis of precisely defined structures [4-6]. Combustion and mechano-chemical techniques offer environmentally sustainable and scalable options. These customized synthesis techniques have improved the performance of ferrites. Spinel ferrites have diverse applications, including gas sensors for detecting toxic and flammable gases like liquefied petroleum gas (LPG), ethanol, methanol, and nitrogen dioxide (NO2); photocatalytic processes for pollutant removal; and energy-related uses in lithium-ion batteries and supercapacitors [7-11].

Spinel ferrites, characterized by the general formula MFe2O4 (where M represents a divalent metal ion such as zinc (Zn), cobalt (Co), nickel (Ni), or manganese (Mn)), have garnered significant interest owing to their remarkable electrical, magnetic, optical, and catalytic capabilities [12]. Recent breakthroughs in spinel ferrites have been notable, especially in the fields of nanotechnology and functional materials research. Research is currently focused on nanostructures, hybrid composites, and doping approaches to enhance the magnetic, electrical, and catalytic properties of materials [12,13]. Nanostructured spinel ferrites, such as hollow spheres, core-shell configurations, and hierarchical morphologies, exhibit increased surface area and enhanced reactivity. Composites using carbon-based elements such as graphene or carbon nanotubes have enhanced electrical conductivity and mechanical stability [4,13]. Advanced doping techniques enable the precise adjustment of optical, magnetic, and gas-sensing characteristics, rendering them adaptable for novel applications.

$ZnFe_2O_4$ is a spinel ferrite compound recognized for its distinctive physical, chemical, magnetic, and electrical characteristics, rendering it appropriate for various applications. $ZnFe_2O_4$ possesses a cubic spinel crystal structure, generally exhibiting a density of approximately 5.3 g.cm^{-3}, and its nanostructured NPs frequently demonstrate a high surface area. It is stable and corrosion-resistant, rendering it appropriate for severe environmental conditions [14,15]. The bandgap of $ZnFe_2O_4$ ranges from 1.9 to 2.0 eV, facilitating visible-light photo catalysis. $ZnFe_2O_4$ has weak magnetic characteristics at ambient temperature owing to its conventional spinel configuration, with zinc ions residing in tetrahedral sites and iron ions in octahedral sites. $ZnFe_2O_4$ is a semiconductor characterized by high resistivity, generally around 104 Ω.m, and a negative temperature coefficient of resistance (TCR), signifying semiconducting properties [16-18]. The activation energy for electrical conduction is moderate, contingent upon synthesis conditions and doping. Its exceptional stability enables successful operation at elevated temperatures, while its gas sensitivity renders it an optimal material for gas sensors. $ZnFe_2O_4$ demonstrates excellent catalytic activity, chemical resilience, and environmental compatibility, rendering it a flexible material for energy, environmental, and sensor applications [8,19].

Liquefied Petroleum Gas (LPG), mostly consisting of propane and butane, is a commonly utilized energy source for cooking, heating, and fueling vehicles. LPG is extremely combustible and can create explosive combinations with air, presenting significant fire and explosion risks. The unregulated emission of LPG exacerbates air pollution and the global warming effect. Although LPG combusts more cleanly than numerous fossil fuels and emits reduced quantities of carbon dioxide and particulate matter, leaks occurring during manufacture, transportation, or utilization might intensify climate change. The risk of ground and water contamination from LPG spills underscores the necessity for vigilant monitoring [20,22]. The origins of LPG leaks encompass defective storage cylinders, pipeline malfunctions, incorrect handling, and unintentional accidents. Inhaling excessive

amounts of LPG can induce dizziness, nausea, respiratory distress, and, in extreme instances, asphyxiation resulting from oxygen displacement. Extended exposure may result in central nervous system impairment [20,21]. The identification and surveillance of LPG are essential to prevent accidents, safeguard human health, and reduce environmental consequences. Prompt identification of leaks facilitates prompt responses, mitigating the risk of fires, explosions, and harmful exposure. Monitoring systems in residential, commercial, and industrial environments improve safety by delivering real-time alerts and facilitating adherence to safety rules. Advanced LPG sensors and detection systems enhance safety in residential and occupational settings while reducing environmental impact [22,23].

This study emphasizes the synthesis, characterization, and gas sensing applications of $ZnFe_2O_4$ NPs produced by economical methods. We synthesized zinc ferrite NPs with a simple and cost-effective precipitation process, ensuring scalability and economic viability while preserving material quality. The NPs were subsequently processed into thick films by a screen-printing technique, providing an economical approach for film manufacturing. The structural, morphological, and chemical characteristics of the $ZnFe_2O_4$ films were meticulously analyzed using sophisticated techniques, including XRD for phase identification, FESEM for surface morphology, EDAX for elemental analysis, UV-Vis spectroscopy for optical bandgap assessment, and FTIR for functional group examination. The gas sensing efficacy of the $ZnFe_2O_4$ films was assessed utilizing a static gas sensing apparatus. The films exhibited remarkable sensitivity and selectivity to LPG.

2. Materials and Methods

2.1. Synthesis of $ZnFe_2O_4$ NPs

All necessary analytical grade (AR) chemicals with 99.99% purity were acquired from Modern Chemicals, Nashik, Maharashtra. All compounds were utilized without additional purification. The co-precipitation approach is frequently employed to synthesize spinel ferrite NPs due to its simplicity and efficacy in producing tiny, homogenous particles [14,24,25]. This approach employs zinc nitrate hexahydrate [$Zn(NO_3)_2 \cdot 6H_2O$] and iron nitrate nonahydrate [$Fe(NO_3)_3 \cdot 9H_2O$] as precursor solutions. Sodium hydroxide (NaOH) is introduced to the aqueous solution to facilitate the development of metal hydroxide precipitates. NaOH functions as a surfactant to inhibit nanoparticle agglomeration. The solution is heated to a reaction temperature of 60°C, after which the precipitate is decanted and washed thrice with distilled water and ethanol to eliminate contaminants and surplus surfactant. The resultant precipitate was filtered using Whatman filter (mesh 41) paper and dehydrated overnight at room temperature. The desiccated particles are further ground in a mortar to attain homogeneity. The resultant powder is calcined at 400°C for 3 h to improve crystallinity and facilitate phase formation, thereby preparing the NPs for characterization.

2.2. Development of Thick Films

Thick films of zinc ferrite ($ZnFe_2O_4$) were fabricated utilizing an economical and portable screen-printing method [26]. The films were deposited on glass substrates (2.5 cm x 1.25 cm). Before deposition, all substrates were methodically cleaned with distilled water and acetone to guarantee a pristine surface and eliminate any contaminants. The generated $ZnFe_2O_4$ NPs were utilized to fabricate the thick films. A 70:30 wt. % ratio of inorganic to organic compounds was utilized for the synthesis of undoped $ZnFe_2O_4$ films. $ZnFe_2O_4$ NPs constituted the inorganic component, whereas butyl carbitol acetate and ethyl cellulose comprised the organic component. Following comprehensive amalgamation of the inorganic and organic constituents, the paste was applied to the glass substrates utilizing a screen-printing apparatus. The deposited films were subjected to drying under an infrared (IR) lamp for 30 to 35 minutes to eliminate solvent residues. The films underwent annealing at 400°C in a muffle furnace for 3 h to improve adhesion, eliminate organics, and enhance crystallinity [26,27]. The produced films were further analyzed employing several standard instruments and procedures to assess their structural, morphological, optical, and gas-sensing capabilities.

3. Results and Discussion

3.1. X-ray Diffraction (XRD) Analysis

XRD analysis is an effective method for ascertaining the crystallographic structure, phase purity, and crystallite dimensions of materials. Figure 1 illustrates the X-ray diffraction pattern of zinc ferrite. The $ZnFe_2O_4$ nanoparticles (NPs) produced via the co-precipitation process exhibits crystallinity and phase purity.

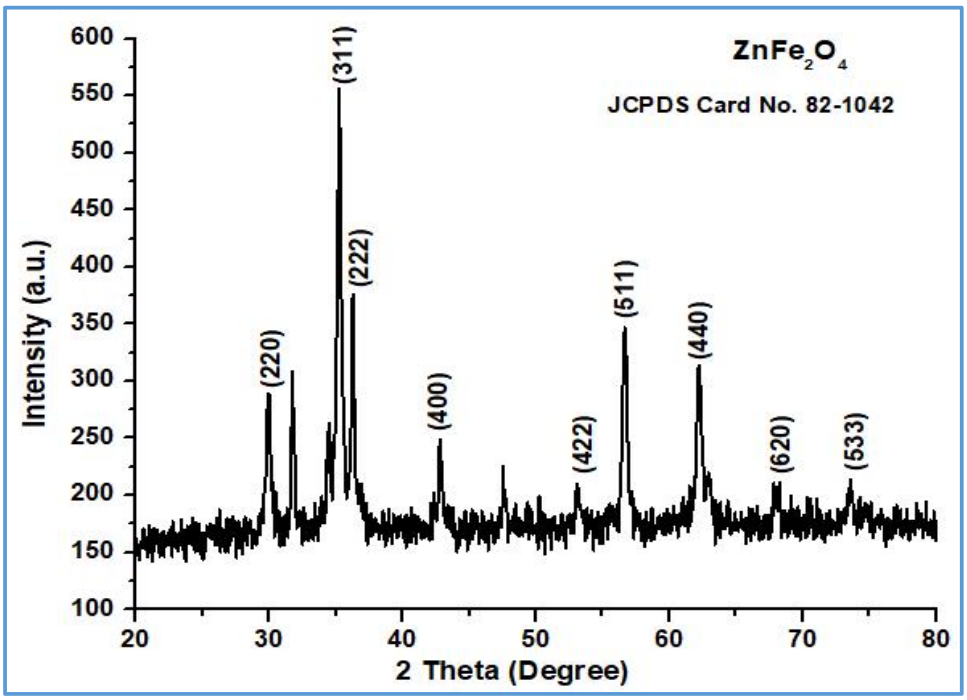

Figure 1: XRD Pattern of Zinc Ferrite Thick Films

The observed diffraction peaks correspond to the spinel cubic structure of $ZnFe_2O_4$ and the peak positions align with the Joint Committee on Powder Diffraction Standards (JCPDS) card no. 82-1042 [28,29]. The notable peaks at 2θ values of roughly 29.9°, 35.3°, 36.9°, 42.9°, 53.2°, 56.6°, 62.1°, and 73.1° are associated with the (220), (311), (222), (400), (422), (511), (440), (620), and (533) crystallographic planes, respectively. The (311) plane demonstrates the greatest intensity, indicative of the spinel ferrite structure. The pronounced and clear diffraction peaks indicate the crystalline characteristics of the NPs. The XRD data validate the successful production of $ZnFe_2O_4$ NPs and underscore the efficacy of the co-precipitation approach in yielding phase-pure and crystalline zinc ferrite [14, 29]. The peak broadening signifies the nanoscale dimensions of the particles. The crystallite size, determined via the Scherrer formula [Eq. 1], was measured at 24.45 nm. (Equation 1)

$$Crystallite\ size\ (D) = \frac{K\lambda}{\beta\ cos\theta} \quad (1)$$

Where, K is constant (0.9–1), β denotes full-width half maxima (FWHM), and θ represents the angle of diffraction. The nanoscale crystallite size significantly enhances the gas-sensing capacity of zinc ferrite [30]. A reduced crystallite size enhances the surface-to-volume ratio, resulting in an expanded active surface area for gas adsorption and interaction. The elevated surface area enhances the material's sensitivity and response time, rendering it appropriate for gas-sensing applications [30,31]. The findings suggest that the produced zinc ferrite NPs, characterized by their nanoscale dimensions and elevated crystallinity, hold potential for the advancement of effective gas sensors.

3.2. Field Emission Scanning Electron Microscopy (FESEM) Analysis

FESEM is an advanced method for examining the surface morphology and nanostructure of materials. Figure 2 displays the FESEM images of zinc ferrite thick films. SEM micrographs illustrates the film's surface shape, exhibiting a porous and granular structure characterized by linked particles, which is crucial for gas sensing applications [32,33]. Figure 2.b presents a detailed examination of the NPs, with particle sizes between roughly 17.54 nm and 28.33 nm. The consistent size distribution and nanoscale diameters of the particles yield a high surface-to-volume ratio, thereby markedly improving the adsorption of gas molecules [33,34].

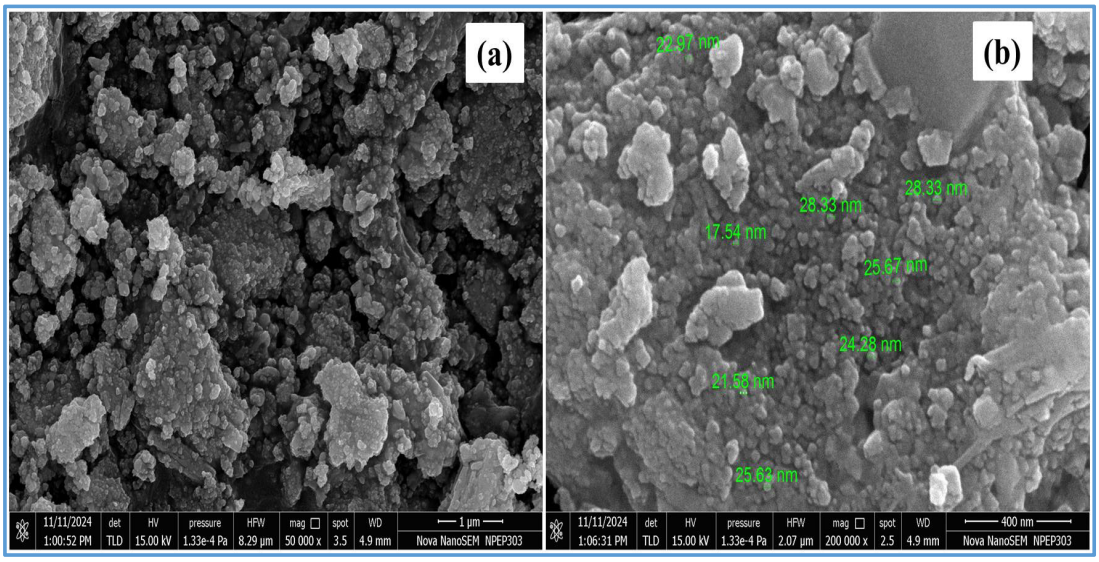

Figure 2: FESEM Images of Zinc Ferrite Thick Films

The porous architecture of the thick films enhances the diffusion of LPG molecules, allowing interaction with adsorbed oxygen on the surface. The nanoscale particle size enhances the density of oxygen chemisorption sites, including vacancies and flaws, hence augmenting the film's sensitivity. The specific surface area is determined via the Brunauer-Emmett-Teller (BET) method (Eq. 2) [35].

$$Specific\ Surface\ Area\ (S_w) = \frac{6}{\rho\, d} \qquad (2)$$

In which, d represents the diameter of a spherical particle, 6 is a constant, and ρ is the density of ZnFe2O4, which is 5.5 g.cm-³.

The surface area was determined to be 3.68 m².g-1. The increased surface area facilitates effective adsorption and interaction with gas molecules, resulting in measurable alterations in the film's resistance and improving its gas sensing capabilities [35,36]. The FESEM results validate that the synthesized zinc ferrite thick films are structurally tailored for superior gas sensing capabilities.

3.3. Energy Dispersive X-ray Analysis (EDAX or EDX)

EDX is an essential technology employed in conjunction with electron microscopy to ascertain the elemental configuration of materials. The EDX spectra of zinc ferrite thick films, seen in figure 3, exhibit typical peaks for the elements zinc (Zn), iron (Fe), and oxygen (O) [36]. The peaks validate the effective synthesis of zinc ferrite NPs by the co-precipitation technique.

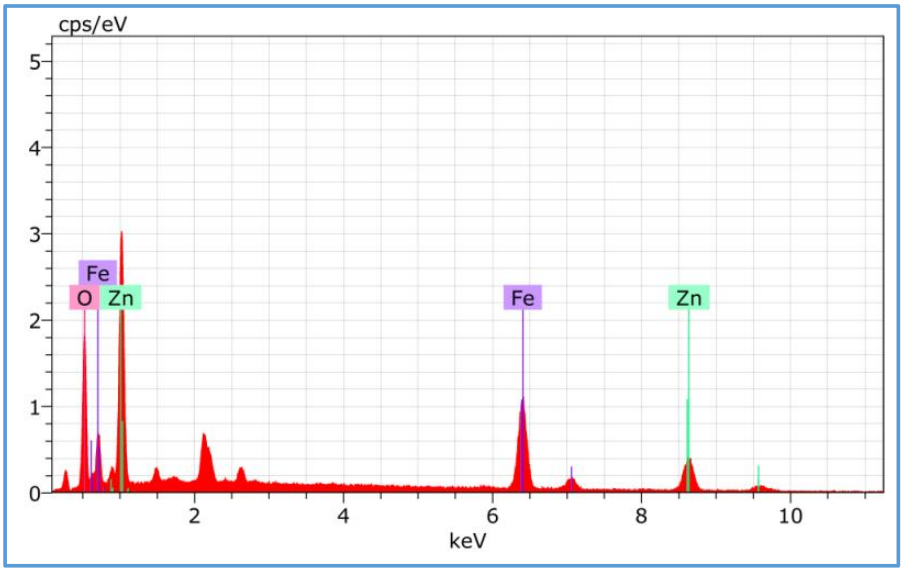

Figure 3: EDX Spectra of Zinc Ferrite Thick Films

The EDX spectra confirm the chemical composition of $ZnFe_2O_4$, demonstrating the successful incorporation of Zn, Fe, and O in the thick layers. The existence of pronounced Zn and Fe peaks, in conjunction with the oxygen peak, indicates the stoichiometric creation of the zinc ferrite structure [36,37]. The co-precipitation approach facilitated the homogeneous amalgamation of zinc and iron precursors during synthesis, resulting in the consistent distribution of these elements within the film. The elemental analysis derived from EDX spectra is presented in Table I.

XRD	**FESEM**	**EDAX**		
Crystallite size (nm)	**Specific surface area (m2.g-1)**	**Element**	Weight (%)	Atomic (%)
24.45	3.68	Zn Fe O	45.80 39.84 14.36	30.31 30.87 38.83

Table I: Structural Results of Zinc Ferrite Thick Films

The oxygen peak in the EDX spectra serves as indirect confirmation of the material's oxygen concentration. Fluctuations in oxygen levels may signify the existence of oxygen vacancies, which are essential for gas detection. Oxygen vacancies augment the chemisorption of oxygen molecules on the surface, generating active sites for interaction with target gas molecules [37, 38]. Oxygen vacancies function as electron donors, altering the material's electrical structure. Upon exposure of $ZnFe_2O_4$ to a target gas, these vacancies promote charge transfer, resulting in a modification of the material's resistance [39].The alteration in resistance supports its gas detecting method [38,39]. The stoichiometry and purity of $ZnFe_2O_4$ were validated by the EDX spectra, guaranteeing reliable gas sensing capability.

3.4. Fourier Transform Infrared (FTIR) Analysis

The FTIR spectra offer detailed insights into the structural and surface properties of materials. Figure 4a illustrates the FTIR spectra of zinc ferrite thick films. The pronounced absorption bands detected in the 400–600 cm^{-1} range correspond to the stretching vibrations of metal-oxygen (M-O) bonds. The band about 540 cm^{-1} is ascribed to the Fe-O stretching vibrations in the octahedral sites of the spinel ferrite structure [40,41]. The band at approximately 440 cm^{-1} corresponds to the Zn-O stretching vibrations in the tetrahedral sites. The broad band in the range of 3300–3500 cm^{-1} corresponds to O-H stretching vibrations, indicating the presence of adsorbed water molecules or surface hydroxyl groups. The feeble absorption band at around 1600 cm^{-1} may relate to the bending vibrations of water molecules or leftover chemical compounds from the manufacturing process [41,42]. The detection of Fe-O and Zn-O vibrations validates the establishment of the $ZnFe_2O_4$ spinel structure, aligning with the anticipated chemical composition. The existence of hydroxyl groups and adsorbed water is crucial for gas sensing applications. These groups augment the contact between gas molecules and the surface, hence enhancing sensitivity. The hydroxyl groups enhance the adsorption and reactivity of gas molecules on the surface. Adsorbed species involved in redox processes modify the electrical conductivity of the material when reducing gases like LPG are present [41-43].

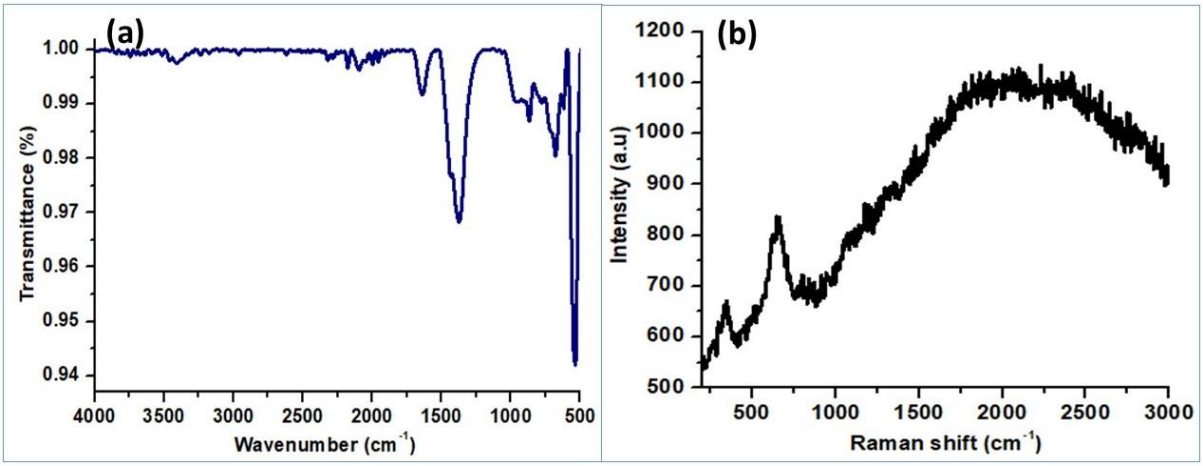

Figure 4: a) FTIR Spectra and b) Raman Spectra of Zinc Ferrite Thick Film

3.6. Raman Spectroscopy Analysis

The Raman spectra of zinc ferrite thick films, illustrated in figure 4b, elucidate the structural and vibrational characteristics of the material. The existence of distinct Raman peaks signifies the spinel structure of $ZnFe_2O_4$, hence affirming its crystalline characteristics and phase purity [44-46]. The vibrational modes correspond to metal-oxygen (Zn–O and Fe–O) bonds inside the spinel lattice, which are crucial for gas adsorption and desorption processes. The peak at around 500 cm^{-1} corresponds to the symmetric stretching mode of the Fe–O bond in tetrahedral coordination. This signifies robust vibrations at tetrahedral sites, typical of spinel ferrites. The peaks between 700 and 800 cm^{-1} correspond to the asymmetric stretching and bending vibrations of oxygen atoms within the $ZnFe_2O_4$ lattice. The spectral range of 1200–2500 cm^{-1} is frequently linked to defect-induced vibrational modes and second-order scattering phenomena. This signifies the existence of structural flaws, oxygen vacancies, and non-stoichiometry, which are pivotal to gas sensing efficacy [47-50].

The structural integrity and vibrational properties shown in the Raman spectra indicate a stable and defect-laden surface for gas sensing. These flaws and oxygen vacancies augment the material's capacity to engage with gas molecules, facilitating efficient adsorption and electron transfer throughout the sensing process [50,51]. The extensive Raman bands signify a level of disorder, which may create additional active sites for gas molecule interaction, hence enhancing the sensor's sensitivity and reaction time.

3.5. Analysis of UV-Visible Spectroscopy

This is an essential instrument for examining the optical characteristics and electronic configuration of spinel ferrites. These materials, recognized for their distinctive magnetic and electrical properties, demonstrate optical absorption in the ultraviolet and visible spectra due to electronic transitions among metal cations located in the octahedral and tetrahedral locations of their spinel lattice [44,45]. Figure 5a illustrates the UV-Visible absorbance spectra of zinc ferrite thick films as a function of wavelength.

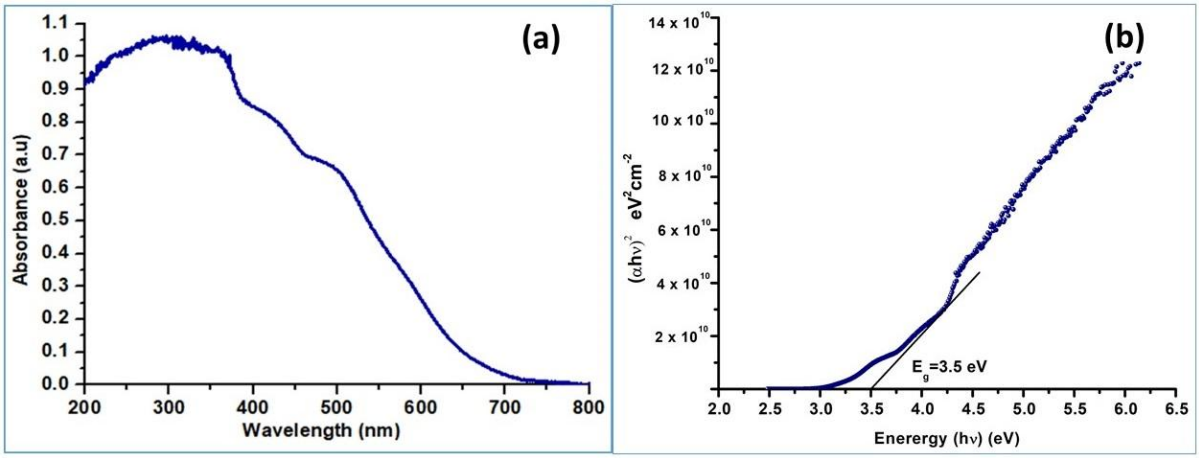

Figure 5: a) Absorbance versus wavelength Spectra and b) Tauc plot of zinc Ferrite Thick Films

The spectrum exhibits significant absorption in the ultraviolet (UV) range of 200–350 nm. The distinctive UV absorption is ascribed to electronic transitions in the zinc ferrite structure, particularly the charge transfer transitions between oxygen anions (O^{2-}) and metal cations (Zn^{2+} and Fe^{3+}). The significant decrease in absorbance at wavelengths over 350 nm signifies the material's absorption edge [45,46]. The optical bandgap (Eg) can be ascertained from this spectrum utilizing the Tauc plot approach (Eq. 3) [47].

$$\alpha = A\,(Eg-h\upsilon)^n/h\upsilon \qquad (3)$$

Where, A represents a constant, Eg is the semiconductor band gap, and 'n' is a numerical value of 1/2 for direct gap compounds and 2 for indirect gap compounds. Figure 5b illustrates the Tauc plot, indicating that the optical band gap energy is around 3.5 eV.

The semiconducting properties of zinc ferrite facilitate efficient surface adsorption and desorption of gas molecules, hence augmenting its sensing abilities. The substantial optical band gap indicates thermal stability, rendering it appropriate for high-temperature gas sensing applications [46-48].

3.7. Electrical Characterization of Zinc Ferrite Thick Films

The electrical characterizations of $ZnFe_2O_4$ thick films were conducted utilizing the half-bridge method and a static electrical characterization device. The resistivity, temperature coefficient of resistance (TCR), and activation energy in lower temperature regions (LTR) and higher temperature regions (HTR) were ascertained by Eqs. 4, 5, and 6, respectively [23, 49-52].

$$\rho = \left(\frac{R \times b \times t}{l}\right) ohm-m \qquad (4)$$

Where, R is resistance of the film at room temperature, t is the thickness of the film, b is breadth of the film, is length of the film.

$$\Delta E = \frac{log\, R}{log\ Ro} \times kT \qquad (5)$$

Where, ΔE is activation energy, R is resistance at higher temperature, Ro is resistance at room temperature, k is Boltzmann constant and T is absolute temperature.

$$TCR = \frac{1}{R_o}\left(\frac{\Delta R}{\Delta T}\right) /^{O} K \qquad (6)$$

Where, ΔR is change in resistance between temperature T_1 and T_2, ΔT is temperature difference between T_1 and T_2 and Ro is resistance of the film at room temperature.

The resistance versus temperature graph of zinc ferrite thick films, depicted in figure 6a, demonstrates the temperature-dependent electrical characteristics of the material. The graph demonstrates a distinct negative temperature coefficient of resistance (NTCR) characteristic, indicating that resistance diminishes with rising temperature [26,27]. This trait is characteristic of semiconducting materials and signifies thermally activated conduction processes. At temperatures between 300 and 350 K, the resistance is markedly elevated, indicating restricted charge carrier mobility and insufficient thermal energy to surmount the activation barrier for conduction.

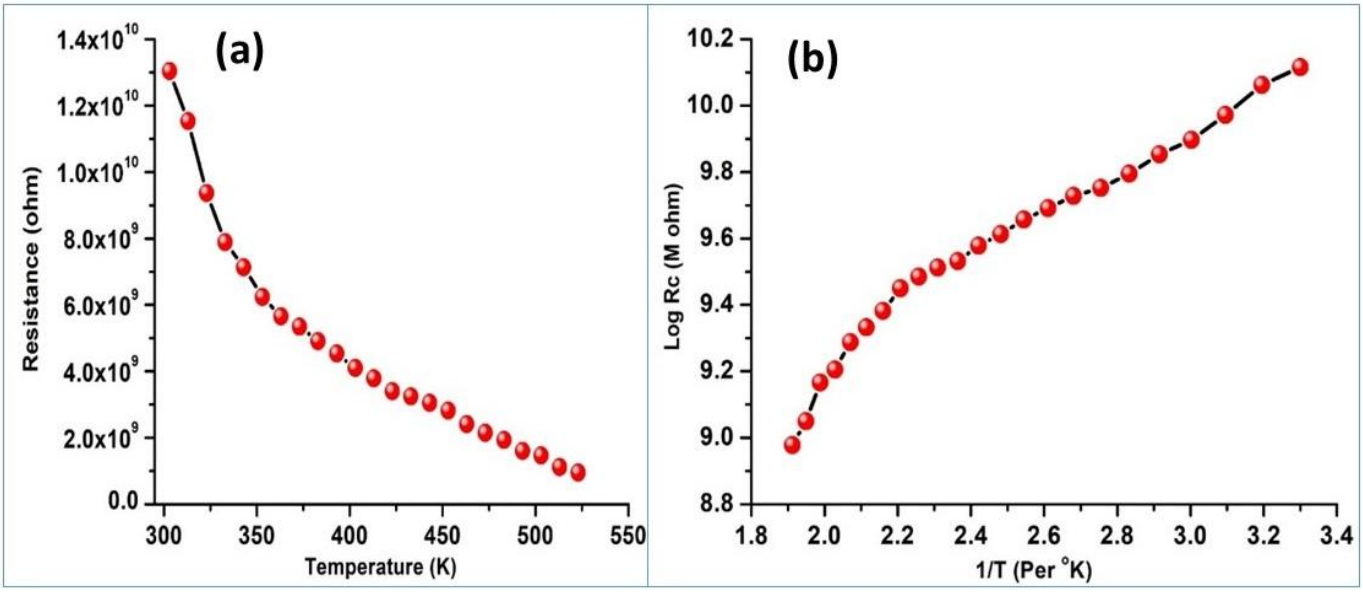

Figure 6: a) Plot of Resistance As A Function Of Temperature And b) Log Rc Versus 1/T Plot of Zinc Ferrite Thick Films

As the temperature increases within the range of 350–500 K, the resistance diminishes dramatically. This behavior indicates that charge carriers (electrons or holes) are thermally excited from the valence band to the conduction band or from donor/acceptor levels into the conduction band. The reduction in resistance with temperature adheres to an Arrhenius-type conduction mechanism, signifying thermally stimulated charge transport [52]. Figure 6b illustrates the Arrhenius plot of zinc ferrite films.

The activation energy is obtained from the slope of the log Rc against 1/T plot, offering insight into the energy necessary for charge carriers to engage in conduction. At elevated temperatures, the oxygen vacancies and adsorbed gas molecules influence the resistivity of $ZnFe_2O_4$ films. The thermal activation energy affects the sensitivity and reaction time of the gas sensor [35,52]. The film thickness was determined via the weight difference method. The projected electrical characteristics of zinc ferrite thick films are presented in Table 2.

Thickness (µm)	Resistivity (Ω.m)	TCR (/°C)	Activation Energy (eV)	
			HTR	LTR
16	104267.8	-0.00191	0.3895	0.1301

Table 2: Electrical Properties of Zinc Ferrite Thick Films

3.8. Characterization of Gas Sensing Properties of Zinc Ferrite Thick Films

The $ZnFe_2O_4$ thick films were assessed for their gas sensing capabilities in the presence of both oxidizing gases (NO_2, CO_2) and reducing gases (LPG, ethanol, CH_4). Gas sensing measurements were conducted utilizing a static gas sensing system engineered to uphold regulated environmental and operational conditions. This system comprised essential elements including a thermocouple for precise temperature monitoring, an electrical coil for correct heating of the sensor material, and a digital temperature indication for real-time temperature regulation. The system utilized a +30 V DC power source to ensure a stable voltage across the sensor element, while a multimeter was employed to document variations in resistance during gas exposure. The configuration included a 25-liter glass dome, functioning as an enclosed chamber for gas exposure, enabling precise control and monitoring of gas concentration. The chamber design facilitated minimum gas leakage and consistent gas distribution, yielding reliable and reproducible results [52-54]. Throughout the sensing procedure, $ZnFe_2O_4$ thick films were subjected to different gases at various temperatures, facilitating the assessment of their gas sensing characteristics. The sensitivity and selectivity of the films were quantified utilizing Equations 7 and 8, respectively [55, 56].

$$Sensitivity\ (\%) = \frac{R_{gas} - R_{air}}{R_{air}}\ x\ 100 \qquad (7)$$

Where, R_{gas} denotes the resistance of the film in the presence of gas, while Rair represents the resistance of the film in air.

In which location, S_{gas} is the sensitivity of the interfering gas at an optimal working temperature, while $S_{target\ gas}$ represents the sensitivity of the target gas at the identical temperature. Figure 7a illustrates a plot of sensitivity in relation to operating temperature for zinc ferrite thick films.

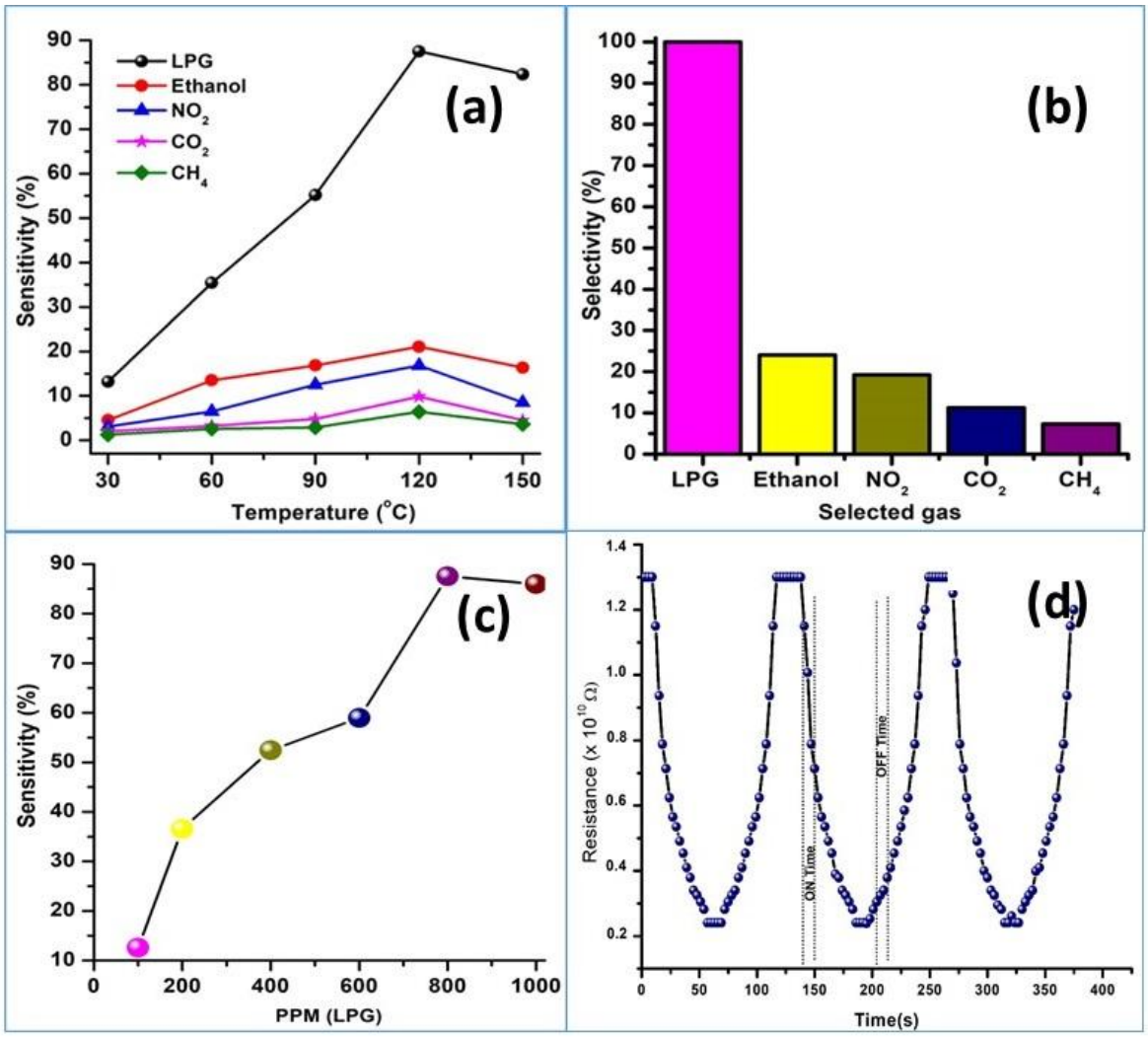

Figure7: a) Plot of Sensitivity Versus Operating Temperature, b) Selectivity Histogram, c) Sensitivity Versus Lpg Gas Concentration, and d) Response and Recovery Plot of Zinc Ferrite Thick Films To Lpg

The $ZnFe_2O_4$ thick films demonstrated a maximum sensitivity of 87.52% to LPG at an ideal temperature of 120°C, underscoring its significant potential for LPG sensing applications. The exceptional sensitivity can be ascribed to various aspects, including the surface chemistry, nanostructure, and electrical characteristics of $ZnFe_2O_4$. At 120°C, the $ZnFe_2O_4$ film surface achieves an ideal equilibrium between gas adsorption and desorption processes, facilitating maximal contact with LPG molecules [56,57]. LPG, as a reducing gas, gives electrons to the sensing material when it interacts with the adsorbed oxygen species on the $ZnFe_2O_4$ surface. This process diminishes the density of adsorbed oxygen ions (O^-, O_2^-) and subsequently elevates the concentration of charge carriers (electrons) in the film, resulting in a substantial reduction in resistance. The spinel structure of $ZnFe_2O_4$ and the presence of oxygen vacancies are crucial in promoting electron transfer processes and improving surface reactivity with LPG molecules. The extensive surface area and porous characteristics of the thick films offer several active sites for LPG adsorption, hence improving the sensor responsiveness of the film. In contrast to oxidizing gases such as NO_2 or CO_2, LPG exhibits a more potent reducing effect on the $ZnFe_2O_4$ surface, leading to a more significant alteration in resistance [56-58]. The sensitivity to LPG is seen to be greater than that of other selected gases, as demonstrated in Fig. 10a. The cause may be attributed to the chemical reactivity of LPG. Figure 7c illustrates the sensitivity of zinc ferrite thick films in relation to LPG gas concentration.

The $ZnFe_2O_4$ thick films exhibited remarkable sensitivity to LPG gas, with a peak sensitivity of 87.52% at an ideal operating temperature of 120°C and an LPG concentration of 800 ppm (Figure 7b). A comparative investigation with different concentrations, including 100, 200, 400, 600, and 1000 ppm, indicated that sensitivity reached its zenith at 800 ppm. The sensitivity demonstrated a decreasing trend both below and beyond this concentration, suggesting that 800 ppm is the ideal level for maximum sensor response [58,59]. This response indicates that the $ZnFe_2O_4$ thick films are highly efficient for detecting LPG at moderate concentrations, rendering them appropriate for practical gas sensing applications.

Figure 7d illustrates the reaction and recovery characteristics of $ZnFe_2O_4$ thick films to liquefied petroleum gas (LPG). The films exhibited a swift response time of 12 seconds and a recovery time of 83 seconds upon exposure to LPG. The rapid reaction and recovery times underscore the efficacy and dependability of $ZnFe_2O_4$ thick films for gas sensing applications [52,60]. The reproducibility of a gas sensor denotes its capacity to yield consistent and dependable findings when subjected to the same gas under same conditions across several testing cycles [60,61]. Figure 7d illustrates the repeatability plot of zinc ferrite thick films.

The film sensor's performance is stable over time, with each test duration spanning 5 days. The reduction in sensitivity over 60 days may be ascribed to various factors, including the slow deterioration of the sensor material and surface contamination. Continuous exposure to gas molecules may result in the slow deterioration of the sensor material. The physical or chemical alterations resulting from extended exposure to LPG. This may lead to a diminished quantity of active sites for gas interaction, hence decreasing the sensor's sensitivity over time. Surface fouling due to frequent exposure to LPG on zinc ferrite thick films may lead to the accumulation of impurities, potentially diminishing the interaction between gas molecules and the active sites of $ZnFe_2O_4$. This fouling impairs the sensor's capacity to detect the gas efficiently [60-63].

4. Conclusion

ZnFe2O4 NPs were produced via the precipitation process. The screen-printing process shown efficacy in the fabrication of $ZnFe_2O_4$ thick films, which were effectively utilized for gas sensing applications. $ZnFe_2O_4$ spinel ferrite has emerged as a promising material owing to its distinctive structural, electrical, optical, and gas-sensing characteristics. The XRD study validated the spinel cubic structure of $ZnFe_2O_4$, with the observed peak locations corresponding to JCPDS card no. 82-1042. The crystallite size was determined to be 24.45 nm via XRD analysis. FESEM results reveal a porous and granular structure characterized by linked $ZnFe_2O_4$ particles. The surface area measured 3.68 m^2/g. The EDX spectra validate the effective synthesis of stoichiometric $ZnFe_2O_4$ thick films, evidenced by the presence of Zn, Fe, and O in the spectrum. The FTIR spectra reveal vibrational bands that validate the spinel structure and indicate the presence of surface hydroxyl groups, which are crucial for the material's application in gas sensing, where surface reactions and oxygen vacancies are integral. The UV analysis reveals a significant absorption in the ultraviolet area spanning 200–350 nm, with an energy band gap measured at 3.5 eV. The Raman analysis verifies that the structural and vibrational characteristics of $ZnFe_2O_4$ thick films are optimal for gas sensing applications, providing stability, elevated surface activity, and efficient charge transfer mechanisms essential for dependable and sensitive gas detection. The optimal operating temperature of 120°C, along with the structural and electrical characteristics of $ZnFe_2O_4$ thick films, establishes ideal circumstances for effective electron transfer and gas interaction, resulting in the greatest recorded sensitivity of 87.52% to LPG. $ZnFe_2O_4$ is a highly promising material for liquefied petroleum gas sensing applications. The films exhibited proficient sensing attributes, especially in their reaction to LPG, characterized by a rapid response time and adequate recovery time. The sensitivity of the $ZnFe_2O_4$ films was remarkable, particularly for their rapid detection abilities.

Acknowledgment

The authors express gratitude to the Department of Physics and the research center of MGV's MSG Arts, Science, and Commerce College in Malegaon, Maharashtra, India, for granting access to laboratory facilities for this research endeavor. The author expresses gratitude to the Department of Physics and CIF at Savitribai Phule Pune University, Pune, India, for the provision of facilities for XRD, FESEM, EDS, UV, FTIR, and Raman characterization.

Funding
The authors disclosed that they did not receive any grants from funding agencies for the current study endeavour, which is entirely self-funded.

Availability of data and materials
Not Applicable.

Ethical approval
Not required.

Declaration of competing interest
The authors declare that they have no known competing financial interests or personal relationships that could have appeared to influence the work reported in this paper.

Reference
1. Comprehensive Environmental Pollution Index (CEPI), (2025) Accessed on 20th January.
2. Common air pollutants and their health effects - NSW Health, (2025) Accessed on 20th January.
3. Exposure & health impacts of air pollution,(2025), Accessed on 20th January.
4. Szotek, Z., Temmerman, W. M., Ködderitzsch, D., Svane, A., Petit, L., & Winter, H. (2006). Electronic structures of normal and inverse spinel ferrites from first principles. *Physical Review B—Condensed Matter and Materials Physics, 74*(17), 174431.
5. Salih, S. J., & Mahmood, W. M. (2023). Review on magnetic spinel ferrite (MFe2O4) nanoparticles: From synthesis to application. *Heliyon, 9*(6).
6. Tatarchuk, T., Bououdina, M., Judith Vijaya, J., & John Kennedy, L. (2016, August). Spinel ferrite nanoparticles: synthesis, crystal structure, properties, and perspective applications. In *International conference on nanotechnology and nanomaterials* (pp. 305-325). Cham: Springer International Publishing.
7. Qin, H., He, Y., Xu, P., Huang, D., Wang, Z., Wang, H., ... & Wang, C. (2021). Spinel ferrites (MFe2O4): Synthesis, improvement and catalytic application in environment and energy field. *Advances in Colloid and Interface Science, 294*, 102486.
8. Mathew, D. S., & Juang, R. S. (2007). An overview of the structure and magnetism of spinel ferrite nanoparticles and their synthesis in microemulsions. *Chemical engineering journal, 129*(1-3), 51-65.
9. Zhao, D. L., Lv, Q., & Shen, Z. M. (2009). Fabrication and microwave absorbing properties of Ni–Zn spinel ferrites. Journal of Alloys and Compounds, 480(2), 634-638.
10. Šutka, A., & Gross, K. A. (2016). Spinel ferrite oxide semiconductor gas sensors. *Sensors and actuators B: chemical, 222*, 95-105.
11. Dastjerdi, O. D., Shokrollahi, H., & Mirshekari, S. (2023). A review of synthesis, characterization, and magnetic properties of soft spinel ferrites. *Inorganic Chemistry Communications, 153*, 110797.
12. Cruz-Franco, B., Gaudisson, T., Ammar, S., Bolarín-Miró, A. M., de Jesús, F. S., Mazaleyrat, F., ... & Valenzuela, R. (2014). Magnetic properties of nanostructured spinel ferrites. *IEEE transactions on magnetics, 50*(4), 1-6.
13. Van Groenou, A. B., Bongers, P. F., & Stuyts, A. L. (1969). Magnetism, microstructure and crystal chemistry of spinel ferrites. *Materials Science and Engineering, 3*(6), 317-392.
14. Vinosha, P. A., Mely, L. A., Jeronsia, J. E., Krishnan, S., & Das, S. J. (2017). Synthesis and properties of spinel ZnFe2O4 nanoparticles by facile co-precipitation route. *Optik, 134*, 99-108.
15. Ž Lazarević, Z., Jovalekić, Č., Milutinović, A., Sekulić, D., Ivanovski, V. N., Rečnik, A., ... & Ž Romčević, N. (2013). Nanodimensional spinel NiFe2O4 and ZnFe2O4 ferrites prepared by soft mechanochemical synthesis. *Journal of Applied Physics, 113*(18).
16. Yadav, R. S., Kuřitka, I., Vilcakova, J., Urbánek, P., Machovsky, M., Masař, M., & Holek, M. (2017). Structural, magnetic, optical, dielectric, electrical and modulus spectroscopic characteristics of ZnFe2O4 spinel ferrite nanoparticles synthesized via honey-mediated sol-gel combustion method. *Journal of Physics and Chemistry of Solids, 110*, 87-99.
17. Thavarani, M., Robert, M. C., Pavithra, N., Saravanan, R., Kannan, Y. B., & Prasath, S. B. (2022). Effect of Ca2+ doping on the electronic charge density and magnetic properties of ZnFe2O4 spinel ferrites. *Journal of Materials Science: Materials in Electronics, 33*(7), 4116-4131.
18. Lima-Tenório, M. K., Tenório-Neto, E. T., Hechenleitner, A. A. W., Fessi, H., & Pineda, E. A. G. (2016). CoFe2O4 and ZnFe2O4 nanoparticles: an overview about structure, properties, synthesis and biomedical applications. *Journal of Colloid Science and Biotechnology, 5*(1), 45-54.
19. Ren, P., Zhang, J., & Deng, H. (2009). Preparation and microstructure of spinel zinc ferrite ZnFe2O4 by Co-precipitation method. *Journal of Wuhan University of Technology-Mater. Sci. Ed., 24*(6), 927-930.
20. Aishwarya, K., Nirmala, R., & Navamathavan, R. (2021). Recent advancements in liquefied petroleum gas sensors: A topical review. *Sensors International, 2*, 100091.
21. Tladi, B. C., Kroon, R. E., Swart, H. C., & Motaung, D. E. (2023). A holistic review on the recent trends, advances, and challenges for high-precision room temperature liquefied petroleum gas sensors. *Analytica Chimica Acta, 1253*, 341033.
22. Dhawale, D. S., Dubal, D. P., More, A. M., Gujar, T. P., & Lokhande, C. D. (2010). Room temperature liquefied petroleum gas (LPG) sensor. *Sensors and Actuators B: Chemical, 147*(2), 488-494.
23. Ab Ghafar, A. S. (2018). Liquefied Petroleum Gas (LPG) leakage detection and monitoring system. *Journal of Science and Technology, 10*(3).
24. Shinde, V. R., Gujar, T. P., Lokhande, C. D., Mane, R. S., & Han, S. H. (2007). Use of chemically synthesized ZnO thin film as a liquefied petroleum gas sensor. *Materials Science and Engineering: B, 137*(1-3), 119-125.
25. Andhare, D. D., Jadhav, S. A., Khedkar, M. V., Somvanshi, S.

B., More, S. D., & Jadhav, K. M. (2020, October). Structural and chemical properties of ZnFe2O4 nanoparticles synthesised by chemical co-precipitation technique. In *Journal of Physics: Conference Series* (Vol. 1644, No. 1, p. 012014). IOP Publishing.
26. Suryawanshi, P. S., Patil, A. V., Padhye, G. G., & Tupe, U. J. (2024). Investigation the influence of calcination temperature on structural, electrical and gas sensing properties MnO2 thick films. *Advanced Materials Research, 1180*, 67-81.
27. Wagh, S. L., Tupe, U. J., Patil, A. B., & Patil, A. V. (2022). Influence of Annealing Temperature on Structural and Electrical Properties of Screen Printed Lanthanum Oxide Thick Films. *Iranian Journal of Materials Science & Engineering, 19*(4).
28. Kumar, G. Y., Naik, H. B., Roy, A. S., Harish, K. N., & Viswanath, R. (2012). Synthesis, optical and electrical properties of ZnFe2O4 nanocomposites. *Nanomaterials and Nanotechnology, 2*, 19.
29. Prasanna, G. D., Jayanna, H. S., & Prasad, V. (2011). Preparation, structural, and electrical studies of polyaniline/ZnFe2O4 nanocomposites. *Journal of Applied Polymer Science, 120*(5), 2856-2862.
30. Wu, K., Li, J., & Zhang, C. (2019). Zinc ferrite based gas sensors: A review. *Ceramics International, 45*(9), 11143-11157.
31. Abdulhamid, Z. M., Dabbawala, A. A., Delclos, T., Straubinger, R., Rueping, M., Polychronopoulou, K., & Anjum, D. H. (2023). Synthesis, characterization, and preliminary insights of ZnFe2O4 nanoparticles into potential applications, with a focus on gas sensing. *Scientific Reports, 13*(1), 19705.
32. Wagner, T., Haffer, S., Weinberger, C., Klaus, D., & Tiemann, M. (2013). Mesoporous materials as gas sensors. *Chemical Society Reviews, 42*(9), 4036-4053.
33. Korotcenkov, G. (2005). Gas response control through structural and chemical modification of metal oxide films: state of the art and approaches. *Sensors and Actuators B: Chemical, 107*(1), 209-232.
34. Jana, R., Hajra, S., Rajaitha, P. M., Mistewicz, K., & Kim, H. J. (2022). Recent advances in multifunctional materials for gas sensing applications. *Journal of Environmental Chemical Engineering, 10*(6), 108543.
35. Patil, A., Tupe, U. J., & Patil, A. V. (2021). Reduced graphene oxide screen printed thick film as NO2 gas sensor at low temperature. *Advanced Materials Research, 1167*, 43-55.
36. Deshmane, V. V., & Patil, A. V. (2020). Cobalt oxide doped hematite as a petrol vapor sensor. *Materials Chemistry and Physics, 246*, 122813.
37. Shakil, M. R., El-Sawy, A. M., Tasnim, H., Meguerdichian, A. G., Jin, J., Dubrosky, J. P., & Suib, S. L. (2018). Single-doped and multidoped transition-metal (Mn, Fe, Co, and Ni) ZnO and their electrocatalytic activities for oxygen reduction reaction. *Inorganic Chemistry, 57*(16), 9977-9987.
38. Al-Hashem, M., Akbar, S., & Morris, P. (2019). Role of oxygen vacancies in nanostructured metal-oxide gas sensors: a review. *Sensors and Actuators B: Chemical, 301*, 126845.
39. Li, J., Na, E., Liang, X., Liang, Q., Fan, M., Chen, H., ... & Zou, X. (2024). Surface oxygen chemistry of metal oxide semiconductors for gas-sensing applications. *Inorganic Chemistry Frontiers, 11*(24), 8602-8626.
40. Rendale, M. K., Mathad, S. N., & Puri, V. (2015). Thick films of magnesium zinc ferrite with lithium substitution: Structural characteristics. *International Journal of Self-Propagating High-Temperature Synthesis, 24*(2), 78-82.
41. Yadav, B. S., Vishwakarma, A. K., Singh, A. K., & Kumar, N. (2023). Oxygen vacancies induced ferromagnetism in RF-sputtered and hydrothermally annealed zinc ferrite (ZnFe2O4) thin films. *Vacuum, 207*, 111617.
42. Deshmane, V. V., Shinde, S., Halwar, D. K., Jain, G., & Patil, A. V. (2022). Tin modified Fe2O3 thick films for monitoring environmental and industrial pollutant gases. *Chemistry Africa, 5*(4), 1069-1082.
43. Halwar, D. K., Deshmane, V. V., & Patil, A. V. (2023). The Combination of Nickel Oxide (NiO) and Molybdenum Trioxide (MoO3) for Pollutant Gas Detection: DK Halwar et al. *Journal of Electronic Materials, 52*(3), 1840-1853.
44. Qiu, J., Wang, C., & Gu, M. (2004). Photocatalytic properties and optical absorption of zinc ferrite nanometer films. *Materials Science and Engineering: B, 112*(1), 1-4.
45. Sutka, A., Strikis, G., Mezinskis, G., Lusis, A., Zavickis, J., Kleperis, J., & Jakovlevs, D. (2012). Properties of Ni–Zn ferrite thin films deposited using spray pyrolysis. *Thin Solid Films, 526*, 65-69.
46. Tanaka, K., Nakashima, S., Fujita, K., & Hirao, K. (2006). Large Faraday effect in a short wavelength range for disordered zinc ferrite thin films. *Journal of applied physics, 99*(10).
47. Johannes, A. Z., Pingak, R. K., & Bukit, M. (2020, April). Tauc Plot Software: Calculating energy gap values of organic materials based on Ultraviolet-Visible absorbance spectrum. In *IOP conference series: materials science and engineering* (Vol. 823, No. 1, p. 012030). IOP Publishing.
48. Kumbhar, S. S., Mahadik, M. A., Mohite, V. S., Hunge, Y. M., Rajpure, K. Y., & Bhosale, C. H. (2015). Effect of Ni content on the structural, morphological and magnetic properties of spray deposited Ni–Zn ferrite thin films. *Materials Research Bulletin, 67*, 47-54.
49. Ravikumar, T., Thirumalaisamy, L., Madanagurusamy, S., & Sivaperuman, K. (2023). Substrate temperature dependent ammonia gas sensing performance of zinc ferrite thin films prepared by spray pyrolysis technique. *Journal of Alloys and Compounds, 959*, 170568.
50. Saritaş, S., Sakar, B. C., Kundakci, M., & Yildirim, M. (2018). The effect of Mg dopants on magnetic and structural properties of iron oxide and zinc ferrite thin films. *Results in Physics, 9*, 416-423.
51. Suresh, S., Rangarajan, S., Bera, S., Krishnan, R., Kalavathi, S., & Velmurugan, S. (2016). Electrochemical characterization of nano zinc ferrite coating on carbon steel by pulsed laser deposition. *Thin Solid Films, 612*, 250-258.
52. Lad, U. D., Kokode, N. S., & Tupe, U. J. (2022). Study of pn heterojunction thin films for reducing gas sensing application fabricated by thermal evaporation technique. *Advanced Materials Research, 1172*, 67-82.

53. Shinde, R. S., Khairnar, S. D., Patil, M. R., Adole, V. A., Koli, P. B., Deshmane, V. V., ... & Patil, A. V. (2022). Synthesis and characterization of ZnO/CuO nanocomposites as an effective photocatalyst and gas sensor for environmental remediation. *Journal of Inorganic and Organometallic Polymers and Materials, 32*(3), 1045-1066.
54. Koli, P. B., Kapadnis, K. H., Deshpande, U. G., Tupe, U. J., Shinde, S. G., & Ingale, R. S. (2021). Fabrication of thin film sensors by spin coating using sol-gel LaCrO3 Perovskite material modified with transition metals for sensing environmental pollutants, greenhouse gases and relative humidity. *Environmental Challenges, 3*, 100043.
55. Koli, P. B., Birari, M. D., Ahire, S. A., Shinde, S. G., Ingale, R. S., & Patil, I. J. (2022). Ferroso-ferric oxide (Fe3O4) embedded g-C3N4 nanocomposite sensor fabricated by photolithographic technique for environmental pollutant gas sensing and relative humidity characteristics. *Inorganic Chemistry Communications, 146*, 110083.
56. Srivastava, R., & Yadav, B. C. (2015). Nanostructured ZnFe2O4 thick film as room temperature liquefied petroleum gas sensor. *Journal of Experimental Nanoscience, 10*(9), 703-717.
57. Chaudhari, P. R., Darunkar, S. S., Bansod, S. M., Gaikwad, V. M., & Acharya, S. A. (2016, May). LPG-sensing characteristics of nanocrystalline ZnFe2O4 synthesized by co-precipitation method. In *AIP Conference Proceedings* (Vol. 1728, No. 1, p. 020460). AIP Publishing LLC.
58. Rezlescu, N., Rezlescu, E., Tudorache, F., & Popa, P. D. (2009). Gas sensing properties of porous Cu-, Cd-and Zn-ferrites. *Romanian Reports in Physics, 61*(2), 223-234.
59. Shinde, V. S., Kapadnis, K. H., Sawant, C. P., Koli, P. B., & Patil, R. P. (2020). Screen print fabricated In3+ decorated perovskite lanthanum chromium oxide (LaCrO3) thick film sensors for selective detection of volatile petrol vapors. *Journal of Inorganic and Organometallic Polymers and Materials, 30*(12), 5118-5132.
60. Shinde, V. S., Kapadnis, K. H., Patil, A. P., & Koli, P. B. (2022). Designing of LaCrO3− TiO2 nanocomposites p: n heterojunction-based sensor material for the selective detection of volatile petrol vapors (PV) and CO2 gas vapors. *Journal of the Indian Chemical Society, 99*(3), 100367.
61. Zhang, L., Tian, F. C., Peng, X. W., & Yin, X. (2014). A rapid discreteness correction scheme for reproducibility enhancement among a batch of MOS gas sensors. *Sensors and Actuators A: Physical, 205*, 170-176.
62. Tupe, U. J., Zambare, M. S., Patil, A. V., & Koli, P. B. (2020). The binary oxide NiO-CuO nanocomposite based thick film sensor for the acute detection of Hydrogen Sulphide gas vapours. *Material Science Research India, 17*(3), 260-269.
63. Sekhar, P. K., Billey, W., Begay, M., Thomas, B., Woody, C., & Soundappan, T. (2024). Sensor reproducibility analysis: challenges and potential solutions. *ECS Sensors Plus, 3*(4), 046401.